Vacuum deposition of $\chi^{(2)}$ nonlinear organic single crystal films on silicon

Nina Krainova*,[1,2] Holly M. Johnson*,[3] Raju Lampande,[1,2] Siyu Gao,[4] Noa Marom,[4,5,6] Barry P. Rand,[3,7] and Noel C. Giebink[1,2]

[1)]*Dept. of Electrical Engineering and Computer Science, University of Michigan, Ann Arbor, MI 48109, USA*
[2)]*Dept. of Electrical Engineering, Pennsylvania State University, University Park, PA 16801, USA*
[3)]*Dept. of Electrical and Computer Engineering, Princeton University, Princeton, NJ 08544, USA*
[4)]*Dept. of Materials Science and Engineering, Carnegie Mellon University, Pittsburgh, PA 15213, USA*
[5)]*Dept. of Physics, Carnegie Mellon University, Pittsburgh, PA 15213, USA*
[6)]*Dept. of Chemistry, Carnegie Mellon University, Pittsburgh, PA 15213, USA*
[7)]*Andlinger Center for Energy and the Environment, Princeton University, Princeton, NJ 08544, USA*

(*Correspondence email address: ngiebink@umich.edu)

Integrating second order nonlinear ($\chi^{(2)}$) optical materials on chip is an ongoing challenge for Si photonics. Noncentrosymmetric molecular crystals have the potential to deliver high $\chi^{(2)}$ nonlinearity with good thermal stability, but so far have been limited to growth from solution or the melt, which are both difficult to control and scale up in manufacturing. Here, we show that large (> 100 μm) single crystal domains of the nonlinear molecule 2-[3-(4-hydroxystyryl)-5,5-dimethylcyclohex-2-enylidene] malononitrile (OH1) can be grown monolithically on either glass or Si via vacuum evaporation followed by a short thermal annealing step. The crystallites are tens of nm thick and exhibit strong second harmonic generation with their primary $\chi^{(2)}$ tensor component lying predominantly in plane. Remarkably, we find that a single domain can grow uninterrupted through nearby channels etched on a Si wafer, which may provide a path to integrate OH1 on Si or Si_3N_4 waveguides for a broad range of $\chi^{(2)}$-based photonic integrated circuit functionality.

The vision of integrating organic materials with high second order optical nonlinearity together with Si photonics (which normally lack $\chi^{(2)}$ due to the inversion symmetry of Si, SiO_2 and Si_3N_4) has been pursued for decades because it offers a versatile, monolithic, and back-end-of-line-compatible path to bring $\chi^{(2)}$ functionality on chip[1,2]. To date, the most widely used approach involves electrically poling nonlinear small molecules within a glassy polymer host matrix[3] (and in some cases without a host matrix[4,5]). However, this approach suffers from limited long-term stability due to orientational relaxation of the molecules over time. Bulk $\chi^{(2)}$ molecular crystals, which are well-established for free space applications, do not suffer from this stability limitation nor do they require high poling fields, but growing crystalline thin films on patterned Si, SiO_2, or Si_3N_4 substrates is a major challenge. Some progress has been made growing from solution[6] and from the melt[7–10]; however, a practical vacuum deposition process that can produce single crystal organic films on-chip has yet to be realized.

Here, we show that large (> 100 μm) single crystal domains of the nonlinear molecule 2-[3-(4-hydroxystyryl) -5,5-dimethylcyclohex-2-enylidene] malononitrile (OH1) can be grown on glass and Si wafers via vacuum thermal evaporation followed by a short thermal annealing step[11,12]. The crystallites are tens of nm thick and are oriented with their (011) plane parallel to the substrate, which makes them strongly birefringent with their primary $\chi^{(2)}$ tensor component lying predominantly in plane. Encouragingly, we find that a single domain can grow uninterrupted through several adjacent, lithographically-defined channels, which may open up a path to exploit OH1 in a variety of $\chi^{(2)}$-based Si photonic device applications such as electro-optic modulation, frequency conversion, and photon pair generation.

The OH1 source material is purchased from Swiss THZ, LLC and used as received. Thin films of OH1 are deposited via vacuum thermal evaporation (base pressure of 10^{-7} Torr) at a rate of $\sim 0.6\ \text{Å}\,\text{s}^{-1}$ onto ambient temperature (100) Si substrates with native oxide as illustrated in Fig. 1a. Note that OH1 is relatively unique among $\chi^{(2)}$ molecular crystal materials in its ability to be melted and thermally evaporated without degrading[13–17]. Other substrates such as glass and quartz are also used, but the results are similar to native oxide/Si.

The resulting films are initially amorphous and appear specular by eye; however, they begin to crystallize spontaneously, forming spherulite domains[11] within ~ 1 week. The crystallization process can be initiated and controlled by annealing the samples on a preheated hot plate in a N_2-filled glovebox immediately following deposition in the adjoining vacuum chamber. Initial film thickness ($20-60$ nm), annealing temperature ($100-130\ ^\circ$C), and time ($60-150$ s) are all important variables for determining the size and quality of OH1 crystallites that grow. Figure 1b shows the result for an initial amorphous film thickness of 25 nm after annealing at $120\ ^\circ$C for 3 minutes. The cross-polarized microscope image displays large, platelet-like crystal domains with an average lateral extent on the order of 300 μm. The domain size is likely related

* These authors contributed equally to this work

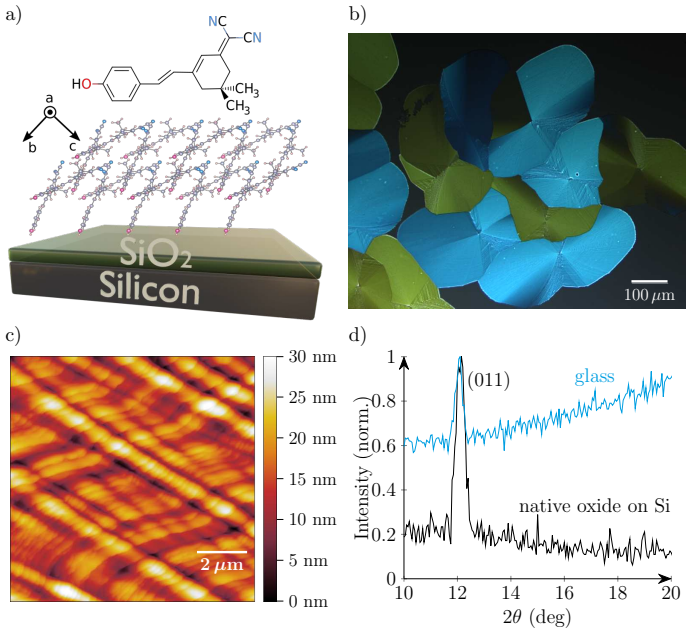

FIG. 1. **(a)** Schematic showing the molecular structure of OH1 and the crystal orientation that results when it is grown and annealed on native oxide/Si. **(b)** Cross-polarized optical microscope image of a crystallized OH1 film with large, platelet-like domains. These crystallites are formed by depositing 25 nm of OH1 on native oxide/Si and annealing the sample at 120 °C for 3 minutes. **(c)** Atomic force micrograph obtained from the center of an OH1 platelet. **(d)** Bragg-Brentano X-ray diffraction scan from a crystallized OH1 film grown on glass and native oxide/Si using Cu K-α radiation. The signal-to-noise ratio of the measurement is low because the film is only ∼25 nm thick.

to the density of nucleation sites (e.g. stray particles) on the wafer surface and could be increased by processing the substrates in a cleanroom environment. At the nanoscale, atomic force microscopy shows evidence of molecular terracing in Fig. 1c. Crystallites such as these are stable under ambient conditions for at least one year (the duration of our experiments) and the crystals are largely preserved after annealing at 85 °C for 24 hrs. This is significant because it supports the potential for long-term stability, which is a primary motivation for pursuing molecular crystals over more technologically-mature poled polymers[7–10].

The crystal growth mechanism is believed to be similar to that of other small molecules studied in Refs.[11] and[12]. Crystallites begin by nucleating at particulates or defects on the substrate. Molecules in the supersaturated amorphous film are mobile enough to rotate and align themselves with the growth front and subsequently incorporate into the crystal. When growth fronts from different nucleation sites meet, a grain boundary is formed.

The X-ray diffraction scan in Fig. 1d exhibits a sharp peak at 12.2°, for both glass and Si substrates. The peak corresponds to reflection from the (011) planes of OH1, indicating that the crystal structure is oriented with its *a*-axis in plane as shown in Fig. 1a. The polarization contrast between crystallites in Fig. 1b therefore reflects their different in-plane *a*-axis orientation. We note that different surface interactions can change the crystal orientation, as OH1 films grown from solution on hydroxyl-functionalized glass have their *a*-axis orthogonal to the substrate due to hydrogen bonding of the OH1 cyano groups with the OH-terminated glass surface[6].

Because the transition dipole moment of OH1 lies predominantly along the *c*-axis, the absorption of individual crystal domains like those in Fig. 1b is highly anisotropic (Fig. 2). Light incident with its polarization along the *a*-axis is absorbed relatively weakly while the orthogonal polarization is strongly absorbed, with a peak absorption coefficient close to 8×10^5 cm^{-1}. Simulations of the absorption spectra of OH1 for light polarized along the *a* and *bc* crystal axes were performed using the GW approximation and Bethe-Salpeter equation (GW+BSE)[18–20] within the framework of many-body perturbation theory, starting from a density functional theory (DFT) mean-field calculation using the Perdew-Burke-Ernzerhof (PBE)[21] functional. Additional computational details are provided in the Supplementary Information. Although the simulated spectra (dashed lines) do not quantitatively reproduce the data, they do capture the high degree of

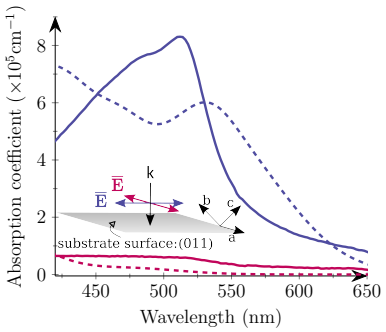

FIG. 2. Absorption coefficient derived from the transmission spectrum of a single OH1 platelet on glass for the two orthogonal polarization orientations depicted in the inset. The dotted lines show corresponding absorption coefficient spectra calculated using GW+BSE@PBE for light polarized along the *bc* (blue) and *a* (red) crystal axes.

anisotropy that is observed, and they help explain the origin of the red shoulder peak (at $\lambda \sim 540$ nm and $\lambda \sim 510$ nm in the simulated and measured spectra, respectively). This shoulder is not observed in solution and results from J-coupling between OH1 molecules in the crystal. Based on previous measurements[22], the crystal is transparent in the near-infrared ($\alpha < 1$ cm^{-1} for $0.7 < \lambda < 1.4$ μm), potentially making it a good option for Si_3N_4 integrated photonics applications at wavelengths <1 μm where many poled polymer nonlinear chromophores strongly absorb[23]. Beyond 1.4 μm, low-level absorption ($\alpha \sim 5$ cm^{-1}) exists due to C-H and O-H vibrational overtones[22].

Second harmonic generation (SHG) is readily observed from individual platelets by focusing fundamental light from an optical parametric amplifier (~ 20 ps pulse width, 1 kHz repetition rate, wavelengths in the range 800-1300 nm) to a spot diameter of approximately 30 μm. Because the silicon substrate absorbs at $\lambda < 1100$ nm, we measure the SHG in reflection mode using a linearly polarized fundamental beam incident at 30°as shown in the inset of Fig. 3a. The reflected SHG is separated from the fundamental with a shortpass filter and detected using a spectrometer. The SHG signal scales quadratically with input power (Fig. 3a) as expected and exhibits a double-lobed polarization pattern (Fig. 3b) that peaks for fundamental polarization parallel to the *bc* plane, which is consistent with the *c*-axis orientation of the dominant $\chi^{(2)}$ tensor component in OH1 crystals[22]. No damage is observed for peak pulse intensities up to 30 GW cm^{-2} at a fundamental wavelength of $\lambda = 900$ nm.

Figure 3c further confirms that the SHG originates from OH1 (as opposed to generic surface SHG) since the resonant enhancement in its action spectrum closely follows the OH1 linear absorption in Fig. 2. Assuming that these OH1 thin films exhibit the same nonlinearity as the bulk OH1 crystals measured in Ref.[22] since their crystal structures are the

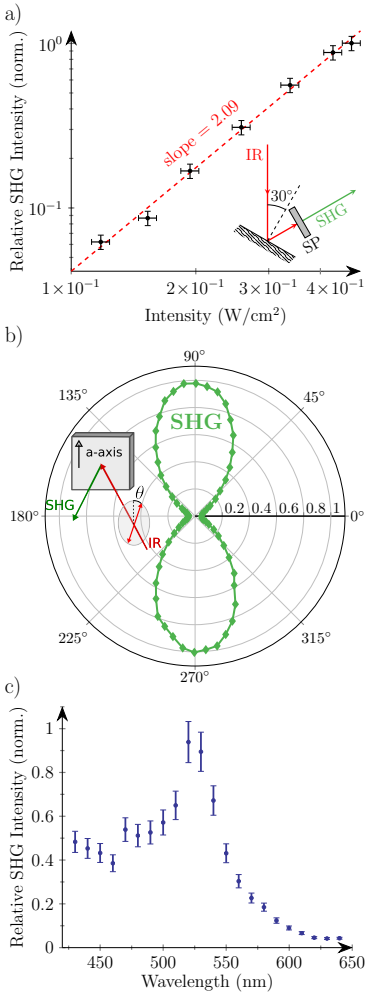

FIG. 3. **(a)** Intensity dependence of second harmonic generation (SHG) measured from a single, 25 nm thick OH1 crystallite on native oxide/Si at a fundamental wavelength of 1100 nm. The inset diagram shows the geometry of the reflection-mode measurement. The fundamental beam is s-polarized parallel to the *bc*-plane of the crystallite. No polarizer is used for the detected SHG. SP: shortpass filter. **(b)** Dependence of SHG intensity on the polarization angle of the fundamental beam, measured relative to the *a*-axis (0°) as illustrated in the inset diagram. **(c)** Action spectrum of the SHG measured by varying the fundamental wavelength from $\lambda = 800$ to 1300 nm. The plot has been corrected for both variation in the fundamental intensity of the optical parametric amplifier and the spectral responsivity of the spectrometer collecting the SHG.

same, the magnitude of the dominant nonlinear coefficient is $d_{33} = 120$ pm V^{-1} at a fundamental wavelength of $\lambda = 1.9$ µm. Given that the nonlinear response increases with decreasing fundamental wavelength (Fig. 3c), this value represents a lower bound for the nonlinear coefficient at telecom wavelengths where, for example, the benchmark material $LiNbO_3$ exhibits $d_{33} = 27$ pm V^{-1} (Ref.[24]).

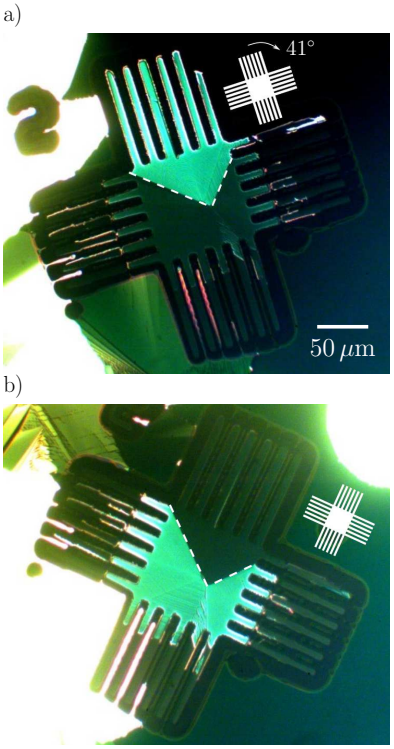

FIG. 4. **(a)** Cross-polarized optical micrograph showing a 25 nm thick OH1 film crystallized in a crossed channel pattern that is etched in 280 nm of thermal oxide on Si. **(b)** The same sample rotated 41°clockwise under the same imaging conditions as indicated by the inset diagrams. The bright green single crystal region that fills the top channels in (a) becomes dark in (b) and gives way to a separate domain that enters the other three sets of channels. The white dashed line highlights the boundary between the two crystallites.

As a first step to understand whether this approach to OH1 crystal growth can be exploited for integrated photonics, we deposit and anneal 20 nm of OH1 on a series of crossed channel patterns etched in 280 µm-thick thermal oxide on Si. This particular pattern is chosen to increase the probability of nucleating crystallites in the large, center area of the pattern so that we can observe whether they grow through the adjacent channels. Remarkably, Fig. 4 shows that this is the case, with a single OH1 crystallite growing uninterrupted through the entire length of multiple parallel channels (Fig. 4a). In these cross-polarized optical microscope images, rotating the sample by 41° reveals two distinct OH1 crystallites separated by a rectangular corner domain boundary (white dashed line). The crystallite highlighted in Fig. 4a fills the full 100 µm length of five adjacent channels; similar crystals are observed for other channel widths ranging down to 5 µm.

If the in-plane orientation of patterned OH1 crystals such as these can be controlled on top of, e.g. a waveguide, it would fix the orientation of the optical indicatrix and $\chi^{(2)}$ tensor, thereby enabling the design of various integrated photonic devices. One route to favor a particular crystal orientation might be to leverage photoalignment layers and related techniques that are used to align liquid crystals in the display industry. Encouragingly in this context, we are able to grow similar size and quality OH1 crystals on top of a 5 nm-thick underlayer of disordered N,N,N',N'-tetrakis(4-methoxyphenyl)benzidine (MeO-TPD) molecules[11,12]. Whether an aligned underlayer can bias the orientation of an OH1 crystal growing on top of it remains an open question for future work.

In summary, we have shown that single crystal thin films of OH1 can be fabricated on Si substrates via vacuum evaporation followed by a short thermal annealing step. Large single crystals grow uninterrupted through nearby lithographically-defined channels that could eventually serve as the arms of, e.g., a push-pull electro-optic modulator. Given that the peak element of the OH1 $\chi^{(2)}$ tensor lies predominantly in plane, integrating these crystals with transverse electric-polarized Si or Si_3N_4 waveguide modes would be a logical choice. While much work remains to demonstrate such a device, the results here at least establish the key ingredients – precisely-controlled vacuum deposition and patterning of a thermally-stable $\chi^{(2)}$ molecular crystal on chip – that are important for a scalable heterogeneous organic-inorganic photonic integration process.

We thank Zhengyang Lyu, Mike Dillender, and Prof. Parag Deotare for assistance with the damage threshold measurement. This work was supported by the National Science Foundation (NSF) Designing Materials to Revolutionize and Engineer our Future (DMREF) program under awards DMR-2323750 (NK, NCG), DMR-2323751 (HMJ, BPR) and DMR-2323749 (SG, NM). This research used resources of the Argonne Leadership Computing Facility (ALCF), which is a DOE Office of Science User Facility supported under Contract DE-AC02-06CH11357 and of the National Energy Research Scientific Computing Center (NERSC), a DOE Office of Science User Facility supported by the Office of Science of the U.S. Department of Energy, under Contract DE-AC02-05CH11231.

SUPPLEMENTARY MATERIAL

See the supplementary material for computational details on the simulated OH1 absorption spectra.

AUTHOR DECLARATIONS

Conflict of Interest

The authors have no conflicts to disclose.

AUTHOR CONTRIBUTIONS

Nina Krainova: Data curation (equal); Writing – original draft (equal); Writing – review & editing (equal). **Holly M. Johnson:** Data curation (equal); Writing – original draft (equal); Writing – review & editing (equal). **Raju Lampande:** Data curation (supporting). **Siyu Gao:** Data curation (supporting); Writing – review & editing (equal). **Noa Marom:** Supervision (equal); Writing – review & editing (equal); Funding Acquisition (equal). **Barry P. Rand:** Supervision (equal); Writing – review & editing (equal); Funding Acquisition (equal). **Noel C. Giebink:** Conceptualization (lead); Supervision (equal); Writing – original draft (equal); Writing – review & editing (equal); Funding Acquisition (equal).

DATA AVAILABILITY

The data that support the findings of this study are available from the corresponding author upon reasonable request.

REFERENCES

[1]J. Leuthold, W. Freude, J.-M. Brosi, R. Baets, P. Dumon, I. Biaggio, M. L. Scimeca, F. Diederich, B. Frank, and C. Koos, "Silicon organic hybrid technology—a platform for practical nonlinear optics," Proceedings of the IEEE **97**, 1304–1316 (2009).

[2]I. Biaggio, "The appeal of small molecules for practical nonlinear optics," Chemistry – A European Journal **28**, e202103168 (2022).

[3]L. R. Dalton, P. A. Sullivan, and D. H. Bale, "Electric field poled organic electro-optic materials: State of the art and future prospects," Chemical Reviews **110**, 25–55 (2010), pMID: 19848381.

[4]Z. Wang, W. Sun, A. Chen, I. Kosilkin, D. Bale, and L. R. Dalton, "Organic electro-optic thin films by simultaneous vacuum deposition and laser-assisted poling," Opt. Lett. **36**, 2853–2855 (2011).

[5]L. Dallachiesa and I. Biaggio, "Electrically poled vapor-deposited organic glasses for integrated electro-optics," Opt. Lett. **47**, 1924–1927 (2022).

[6]S.-J. Kwon, C. Hunziker, O.-P. Kwon, M. Jazbinsek, and P. Günter, "Large-area organic electro-optic single crystalline thin films grown by evaporation-induced local supersaturation with surface interactions," Crystal Growth & Design **9**, 2512–2516 (2009).

[7]A. Hermans, S. Clemmen, R. Baets, J. Genoe, and C. Rolin, "Growth of organic crystalline thin films with strong second-order nonlinearity for integrated optics," (2019).

[8]H. Figi, M. Jazbinšek, C. Hunziker, M. Koechlin, and P. Günter, "Electro-optic single-crystalline organic waveguides and nanowires grown from the melt," Opt. Express **16**, 11310–11327 (2008).

[9]D. Korn, M. Jazbinsek, R. Palmer, M. Baier, L. Alloatti, H. Yu, W. Bogaerts, G. Lepage, P. Verheyen, P. Absil, P. Guenter, C. Koos, W. Freude, and J. Leuthold, "Electro-optic organic crystal silicon high-speed modulator," IEEE Photonics Journal **6**, 1–9 (2014).

[10]H. Figi, D. H. Bale, A. Szep, L. R. Dalton, and A. Chen, "Electro-optic modulation in horizontally slotted silicon/organic crystal hybrid devices," J. Opt. Soc. Am. B **28**, 2291–2300 (2011).

[11]M. A. Fusella, S. Yang, K. Abbasi, H. H. Choi, Z. Yao, V. Podzorov, A. Avishai, and B. P. Rand, "Use of an underlayer for large area crystallization of rubrene thin films," Chemistry of Materials **29**, 6666–6673 (2017).

[12]J. T. Dull, Y. Wang, H. Johnson, K. Shayegan, E. Shapiro, R. D. Priestley, Y. H. Geerts, and B. P. Rand, "Thermal properties, molecular structure, and thin-film organic semiconductor crystallization," The Journal of Physical Chemistry C **124**, 27213–27221 (2020).

[13]M. Jazbinsek and P. Günter, "6 - molecular crystals and thin films for photonics," in *Handbook of Organic Materials for Electronic and Photonic Devices (Second Edition)*, Woodhead Publishing Series in Electronic and Optical Materials, edited by O. Ostroverkhova (Woodhead Publishing, 2019) second edition ed., pp. 177–210.

[14]B. Ruiz, M. Jazbinsek, and P. Günter, "Crystal growth of dast," Crystal Growth & Design **8**, 4173–4184 (2008), https://doi.org/10.1021/cg8003432.

[15]Z. Yang, L. Mutter, M. Stillhart, B. Ruiz, S. Aravazhi, M. Jazbinsek, A. Schneider, V. Gramlich, and P. Günter, "Large-size bulk and thin-film stilbazolium-salt single crystals for nonlinear optics and THz generation," Adv. Funct. Mater. **17**, 2018–2023 (2007).

[16]J.-H. Jeong, B.-J. Kang, J.-S. Kim, M. Jazbinsek, S.-H. Lee, S.-C. Lee, I.-H. Baek, H. Yun, J. Kim, Y. S. Lee, J.-H. Lee, J.-H. Kim, F. Rotermund, and O.-P. Kwon, "High-power broadband organic thz generator," Scientific Reports **3** (2013), 10.1038/srep03200.

[17]M. Fujiwara, M. Maruyama, M. Sugisaki, H. Takahashi, S.-i. Aoshima, R. J. Cogdell, and H. Hashimoto, "Determination of the d-tensor components of a single crystal of n-benzyl-2-methyl-4-nitroaniline," Japanese Journal of Applied Physics **46**, 1528 (2007).

[18]M. Rohlfing and S. G. Louie, "Electron-hole excitations and optical spectra from first principles," Physical Review B **62**, 4927 (2000).

[19]S. Sharifzadeh, "Many-body perturbation theory for understanding optical excitations in organic molecules and solids," J. Phys. Condens. Matter **30**, 153002 (2018).

[20]X. Blase, I. Duchemin, D. Jacquemin, and P.-F. Loos, "The bethe–salpeter equation formalism: From physics to chemistry," The Journal of Physical Chemistry Letters **11**, 7371–7382 (2020).

[21]J. P. Perdew, K. Burke, and M. Ernzerhof, "Generalized gradient approximation made simple," Phys. Rev. Lett. **77**, 3865 – 3868 (1996).

[22]C. Hunziker, S.-J. Kwon, H. Figi, F. Juvalta, O.-P. Kwon, M. Jazbinsek, and P. Günter, "Configurationally locked, phenolic polyene organic crystal 2-{3-(4-hydroxystyryl)-5,5-dimethylcyclohex-2-enylidene}malononitrile: linear and nonlinear optical properties," J. Opt. Soc. Am. B **25**, 1678–1683 (2008).

[23]H. Xu, Y. Sun, Y. Kan, and K. Gao, "Recent progress in design of organic electro-optic materials with ultrahigh electro-optic activities," Chinese Journal of Chemistry **40**, 3001–3012 (2022).

[24]A. Boes, L. Chang, C. Langrock, M. Yu, M. Zhang, Q. Lin, M. Lončar, M. Fejer, J. Bowers, and A. Mitchell, "Lithium niobate photonics: Unlocking the electromagnetic spectrum," Science **379**, eabj4396 (2023), https://www.science.org/doi/pdf/10.1126/science.abj4396.